RESEARCH ARTICLE | JANUARY 12 2026

Anomalous low-field magnetoresistance in Fe_3Ga_4 single crystals

Michelle E. Jamer ; Gregory M. Stephen ; Brandon Wilfong ; Radhika Barua ; Frank M. Abel ; Steven P. Bennett ; Joseph C. Prestigiacomo ; Don Heiman ; Dave Graf

Appl. Phys. Lett. 128, 022402 (2026)
https://doi.org/10.1063/5.0304810
CHORUS

Applied Physics Letters ARTICLE pubs.aip.org/aip/apl

Anomalous low-field magnetoresistance in Fe_3Ga_4 single crystals

Cite as: Appl. Phys. Lett. **128**, 022402 (2026); doi: 10.1063/5.0304810
Submitted: 30 September 2025 · Accepted: 19 December 2025 ·
Published Online: 12 January 2026

Michelle E. Jamer,[1,a)] Gregory M. Stephen,[2] Brandon Wilfong,[1] Radhika Barua,[3] Frank M. Abel,[1] Steven P. Bennett,[4] Joseph C. Prestigiacomo,[4] Don Heiman,[5,6] and Dave Graf[7]

AFFILIATIONS

[1]Physics Department, United States Naval Academy, Annapolis, Maryland 21402, USA
[2]Laboratory for Physical Sciences, College Park, Maryland 20740, USA
[3]Mechanical and Nuclear Engineering, Virginia Commonwealth University, Richmond, Virginia 23220, USA
[4]Materials Science and Technology Division, U.S. Naval Research Laboratory, Washington, District of Columbia 20375, USA
[5]Physics Department, Northeastern University, Boston, Massachusetts 02115, USA
[6]Plasma Science and Fusion Center, MIT, Cambridge, Massachusetts 02139, USA
[7]National High Magnetic Field Laboratory, Florida State University, Tallahassee, Florida 32306, USA

[a)]**Author to whom correspondence should be addressed:** jamer@usna.edu

ABSTRACT

Fe_3Ga_4 possesses a helical spin spiral with a complex competition between ferromagnetic and antiferromagnetic ground states. This competition generates multiple metamagnetic transitions that are governed by both the applied magnetic field and temperature. At intermediate temperatures between T_1 (68 K) and T_2 (360 K), the ferromagnetically aligned spins transition to an antiferromagnetic spin spiral. In this study, magnetoresistance (MR) measurements are performed on an aligned single crystal and compared to magnetization properties in order to gain insight into the unique alignment of the spins. The high-field MR is positive at low temperatures, indicating cyclotronic behavior, and negative at high temperatures from electron–magnon scattering. Of particular significance is a large anomalous positive MR at low fields, possibly due to emergent spin fluctuations, thus prompting further exploration of this multifaceted material.

Published by AIP Publishing. https://doi.org/10.1063/5.0304810

There is a crucial need to explore magnetic materials with novel magnetic transitions to keep pace with the demands of an increasingly digital society.[1] One material of interest has been FeRh for a variety of studies due to its antiferromagnetic (AFM) to ferromagnetic (FM) transition near room temperature. AFM-to-FM transitions are rather rare in materials, and FeRh has been proposed for a variety of applications, including devices that use magnetization as a state variable and logic.[2–5] While this compound has been used as a test bed for possible devices,[6,7] FeRh is hindered by the expensive Rh component, the structural transition accompanying the magnetic transition that can increase brittleness, and the sensitivity of the transition temperature to material quality.

Fe_3Ga_4 has recently been explored as a compound similar to FeRh due to its metamagnetic transitions, but Fe_3Ga_4 has the additional feature of a helical spin spiral (HSS) phase.[8–11] Like FeRh, Fe_3Ga_4 is metallic with a metamagnetic transition near room temperature ($\approx$ 360 K) but without the accompanying structural transitions. The compound forms in the monoclinic C2/m structure with four unique Fe atoms, which allows for the helical spirals with crystallographic information in the supplemental material. Fe_3Ga_4 has two magnetic transitions of interest, which are both sensitive to applied magnetic field and temperature. At $T_1 = 68$ K, the system transitions from a low-temperature FM state to a helical spin spiral (HSS) AFM state, while at $T_2 = 360$ K, the system transitions from the HSS-AFM back to the FM state as illustrated in Fig. 1(a). The magnetic transitions are caused by a sensitive competition between ground state energies of the FM and HSS-AFM structures, where small energy changes cause a change in the magnetic structure.

Some original studies of Fe_3Ga_4 focused on the metamagnetic transition T_1 and the effects of chemical dopants.[8,12] Recently, single crystal studies have been aimed at understanding the configuration of the spin system.[9,10,13] Part of the renewed interest is due to the identification of a topological component in the Hall effect measurements.[10,14] In these newer studies, the magnetic and resistivity properties have been studied.[15] The magnetic properties along each crystallographic direction demonstrate that there is an HSS-AFM state sandwiched between two FM states. The magnetic transitions vary as a function of

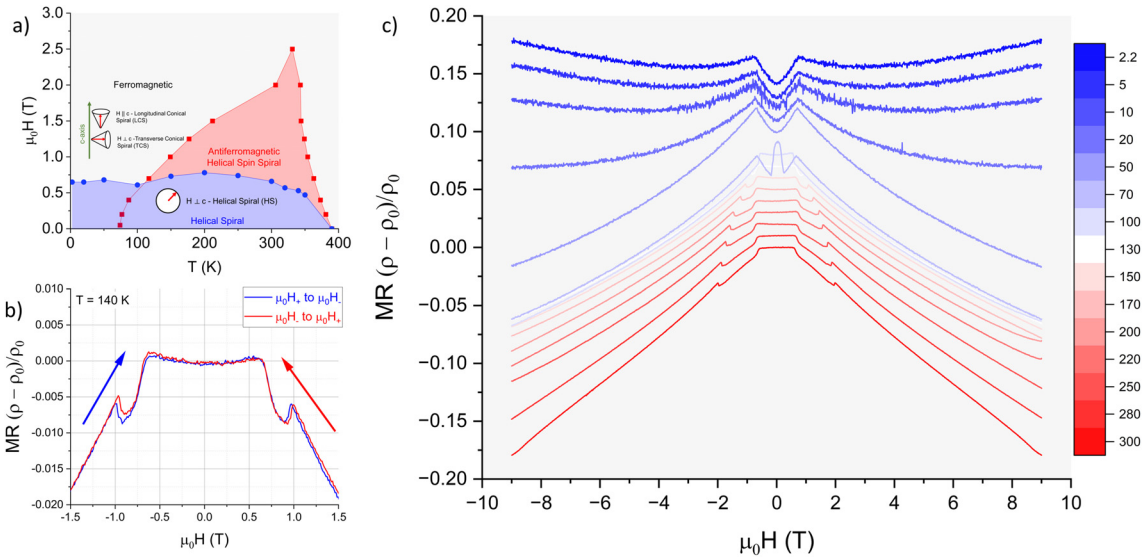

FIG. 1. (a) The magnetic phase diagram with applied field (μ_0 H) and temperature. The antiferromagnetic state is shown in red, where the red region is given by the change in the magnetic transitions T_1 and T_2. The values noted in the diagram are from the *b*-axis as noted in the supplementary material. The helical spiral (HS) in the diagram in blue is the magnetic step along the *b*-axis, where the low-field behavior is a two-dimensional spin spiral. The HS is also observed along the *a*-axis in the antiferromagnetic region as noted in the supplementary material. (b) The magnetoresistance (MR) along the *b*-axis at T = 140 K, where the crystal is in the antiferromagnetic state. The down sweep is in red and the up sweep is in blue. There is a hysteresis observed at μ_0 H ≈ ± 1.0 T, which relates to saturation at T = 140 K. There is a smaller change close to ≈0.75 T, which is the field where the HS transitions to the TCS. (c) The MR at each temperature along the *b*-axis starting from 2.2 to 300 K with offsets with each dataset for ease of viewing of the changes. All data from 2.2 to 300 K and 350 to 65 K are shown in the supplementary material.

both field and temperature, as visualized in the magnetic phase diagram in Fig. 1(a) with full information regarding transition temperatures and fields in the supplementary material. As seen in the magnetic phase diagram, along the *a*- and *b*-axes, the magnetization behaves as a two-dimensional helical spiral in the low-field range ($\mu_0 H \leq 0.75$ T), then transitions into conical magnetic structures at higher fields.

In this work, magnetoresistance (MR) measurements are used in order to understand the coupling between the electrical transport behavior and the magnetic phase properties. These measurements can give more insight into the magnetic coupling in the HSS-AFM state, as well as how these states could be utilized in a practical device. While many AFM-based states are insulators, the spin spiral ordering allows for retained metallicity at room temperature. In this paper, we investigate the crystallographic axes-dependent transport and magnetotransport properties, leading to a deeper understanding of the spin structure. Of particular curiosity is the MR ($MR = \frac{\rho_H - \rho_0}{\rho_0}$) along the *b*-axis, which has a hysteretic MR in the AFM region as the spin structure changes from helical spiral (HS) to transverse conical spiral (TCS) [Fig. 1(b)]. Additionally, a large anomalous positive MR (pMR) emerges at low magnetic fields and low temperatures, as shown in Fig. 1(c). This pMR persists up to nearly room temperature at a reduced magnitude. The data in Fig. 1(c) have been offset by a small constant to improve readability, and all temperatures in the dataset between 2.2 and 300 K are plotted in the SM. The anomalous pMR at low fields correlates with a large electron mobility, which is typically only identified at high fields for FM materials and can indicate helical ordering at low fields.

Single crystals of Fe_3Ga_4 were synthesized using a chemical vapor transport (CVT) method, which was adapted from previous work.[16] Detailed synthesis methods and preliminary properties are described in a prior publication.[10] The transport properties were measured at the National High Magnetic Field Laboratory (NHMFL) DC Field Facility. The MR data were taken between 0 and 9 T and from 2.2 to 300 K, as shown in Fig. 2.

The MR data differ when the field ($\mu_0 H$) is applied parallel to the *a*-, *b*-, and *c*-axes, as seen in Figs. 2(a)–2(c), respectively. The low-field MR data ($\mu_0 H \leq 1.2$ T) for the *a* and *b* crystallographic axes are highlighted in the insets of Figs. 2(a) and 2(b). Most interesting is the *b*-axis data, where there is a strong anomalous pMR at low fields and low temperatures, yet remains small and persistent even up to room temperature. Interestingly, around the metamagnetic transition (T ≈ 75 K), there is no pMR in the low-field region. The MR data are modeled in two magnetic field regions, which are labeled as ρ_{low} and ρ_{high}. The entire field and temperature range can be fit using the following expression:

$$\frac{\rho_H - \rho_0}{\rho_0} = \rho_{low} + \rho_{high}, \tag{1}$$

and examples of the fit is seen in Fig. 2(d).

The low-field component ρ_{low} is a region of anomalous pMR, which is large at low temperatures (T ≤ 75 K) along the *b*-axis. The low-field component corresponds to the field range $\mu_0 H \leq 0.75$ T, where the *a* and *b* axes are in the HS spiral phase as seen in Fig. 1(a). The low-field data described by ρ_{low} provide additional insight into the magnetic structure of Fe_3Ga_4. Along the *b*-axis, ρ_{low} is large at all temperatures below 75 K, and reappears at all temperatures below 300 K with the exception of 75 K. Along the *a*-axis, a similar pMR feature emerges in the temperature range 100 K ≤ *T* ≤ 250 K, matching the

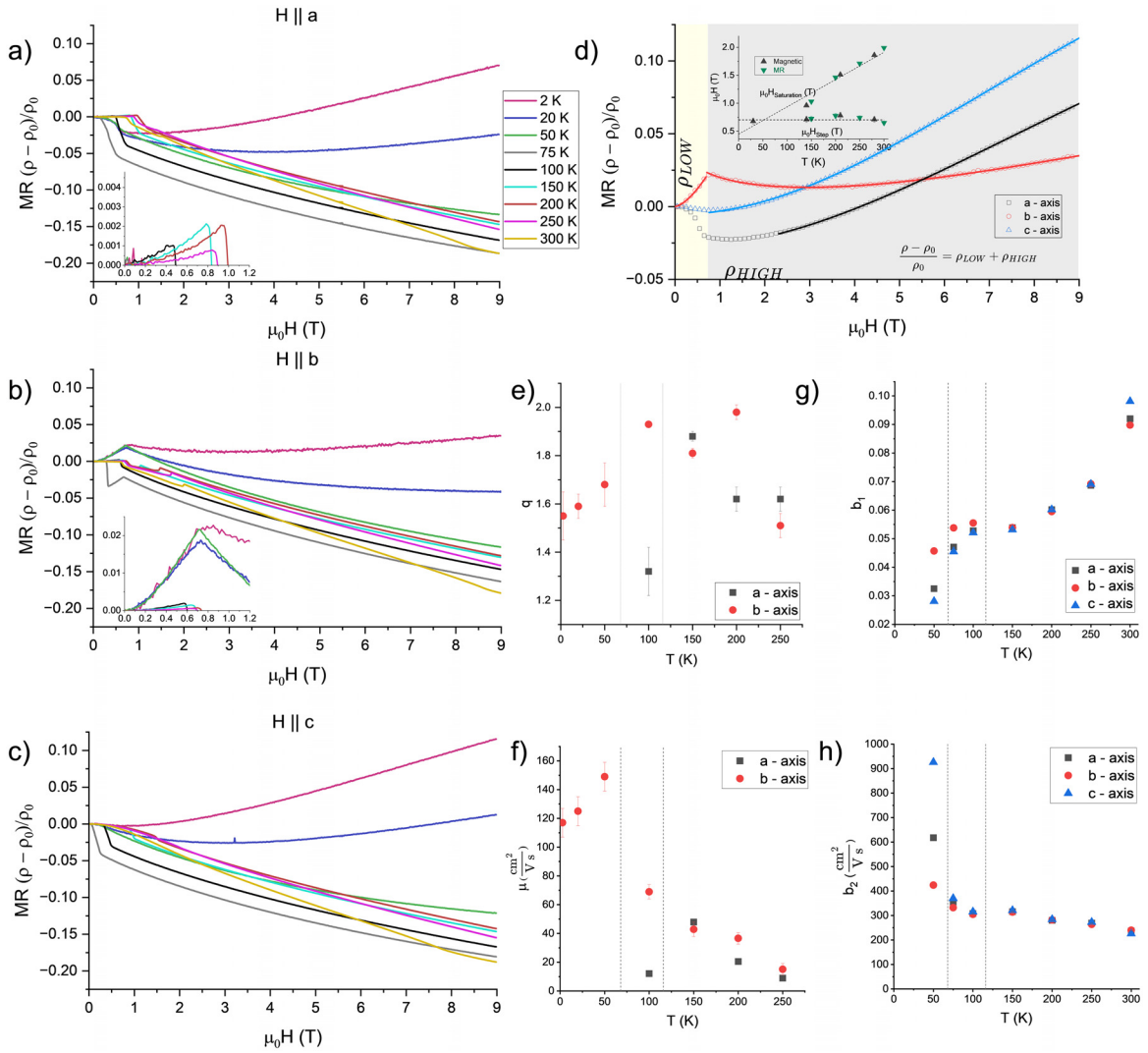

FIG. 2. The data for the magnetoresistance (MR) when $\mu_0 H$ is applied along the (a) *a*, (b) *b*, and (c) *c* crystallographic axes. In the insets in (a) and (b), the data are the same but focused on the region when $\mu_0 H = 0 - 1.2$ T. The data show that the MR along the *b*-axis has a persistent positive contribution below 0.75 T for all temperatures with the exception of the 75 and 300 K data. The *a*-axis has a slight positive magnetoresistance for temperatures when the crystal is in its helical spin spiral (HSS) state after T_1 above 75 K and below 300 K. The legend for temperatures corresponds to all curves on the left side of the figure. (d) An example of the fits for the *a*-, *b*-, and *c*-axes at 2.6 K as noted by solid lines, and the regions for designated field ranges are noted by different colors (ρ_{low} is light yellow and ρ_{high} is light gray). (Inset) The field where saturation occurs and the magnetic step indicating a change from the HS state to the transverse conical spiral (TCS) state along the *b*-axis. Magnetic data describe the data extrapolated from SQUID magnetometry, and MR data are the field where the MR decreases in the intermediate field and temperature range. (e) and (f) The fitting values from modeling the low-field positive magnetoresistance where $MR = (\mu\mu_0 H)^q$, where $1 < q < 2$. The positive magnetoresistance is found along both the *a*-axis (between 75 and 300 K, when the magnetization along this axis is in its TCS state) and *b*-axis (for every temperature other than 75 and 300 K). The dashed vertical gray lines note the temperature for the T_1 transition at 0 T (68 K) and 0.75 T (116 K). (g) and (h) The values from modeling the high-field data that were fit to the electron–magnon model, where $\mathrm{MR} = -b_1 \ln(1 + b_2^2(\mu_0 H)^2)$ for the *a*-, *b*-, and *c*-axes.

behavior observed for the *b*-axis within the TCS magnetic state. The fitted μ values for the *a*- and *b*-axes are also similar in this temperature interval, as shown in Fig. 2(f). However, at 100 K, the μ values for the two crystallographic directions differ significantly. The discrepancy occurs because the metamagnetic transition at 0.75 T takes place at 116 K, indicating that the *a*- and *b*- axes are in the process of entering the TCS state at 100 K. There is no similar positive magnetoresistance at temperatures measured with a magnetic field below 0.75 T along the *c*-axis. We note that pMR at low fields is a characteristic of AFM materials, and we used the following empirical equation:

$$\rho_{low} = (\mu\mu_0 H)^q, \tag{2}$$

where $1 < q < 2$ and μ correlates with the mobility of the carriers.[17–19] A purely linear pMR in AFMs and density wave materials, such as Cr[23]

and 2H-$NbSe_2$,[24] would generally arise from partially gapped Fermi surfaces.[25] Interestingly, the behavior follows a semi-quadratic model associated with s–d scattering.[20–22] When the field is parallel to the spins of one sublattice, fluctuations in that sublattice may be suppressed, while those in the other sublattice may increase. Since the effect is seen below 0.75 T, when the magnetization is in the HS state, the positive MR is most likely due to spin fluctuations as proposed by the Rivier and Zlatic model.[26,27] A normal ferromagnet at 2 K has a relatively low mobility of $< 50\ cm^2/Vs$ and ferromagnets with interesting topological properties normally have large mobilities with large MR, as in the case of MnBi, which has a large mobility of $5000\ cm^2/Vs$ and a positive MR of 250% at 2 K.[28] The mobility of Fe_3Ga_4 in its low-field and low-temperature state has a mobility that is approximately 30 times larger than a regular ferromagnet at 50 K with a mobility of $\approx 150\ cm^2/Vs$ at low fields with a small positive MR. This is particularly interesting since topological and helical materials have a positive MR with a large mobility due to smaller effective masses.[29–31] Due to the size of the mobility and the anomalous pMR at low fields, we expect that the state that has traditionally been attributed to traditional FM order may have helical processions.

The data for the fit for ρ_{low} are seen in Figs. 2(e) and 2(f). In the figure, two temperatures are noted by vertical gray lines, which note where T_1 is located in the metamagnetic transition with no applied field (68 K) and with 0.75 T (116 K). The data for 75 K are not noted since near the transition temperature, there is no positive component, since this temperature correlates with the metamagnetic transition. The data below 68 K increase linearly for the μ and q fitting factor along the b-axis and then decrease. When $T \geq 100$ K, the a-axis has a similar spin structure to the b-axis. The low-field MR along the a-axis moves from negative to positive, where the mobility is 10 times smaller than along the b-axis. The disparity emerges because the metamagnetic transition T_1 occurs near 100 K. However, the data for the a-axis match well after this temperature (well beyond the transition temperature) for both the mobility μ and the exponent q. Since both the a- and b-axes demonstrate helical spiral ordering at low fields beyond the metamagnetic transition as noted by Fig. 1(a), it is reasonable that their fitted values would be similar in the temperature region $150 \leq T \leq 250$ K. There is no positive low-field MR at room temperature (300 K), where the compound is moving toward its ferromagnetic alignment with an applied field.

Along the b-axis, there is a notable decrease in the MR between $0.75 \leq \mu_0 H \leq 3$ T when $T \geq 75$ K. When measuring above the HS to TCS transition ($T_1 \approx 70$ K) there is a step-like behavior where the MR becomes more negative. The magnetic field step and magnetic saturation along the b-axis are both noted in the inset of Fig. 2(d). The field where the decrease in resistance starts is noted by $\mu_0 H_{Step}$, and is ≈ 0.75 T for all temperatures. The resistance increases again when the magnetic state changes from the transverse conical spiral to the ferromagnetic state when the field saturates the compound, as noted by $\mu_0 H_{Saturation}$ in Fig. 2(d) inset. Interestingly, the main hysteresis locations observed in Fig. 1(b) from the field up from −9 T (blue) and down from +9 T (red) correlate with the magnetic ordering change from HS to TCS at 0.75 T. The second hysteresis field location occurs at ± 1.0 T, which is the saturation field at that temperature. After saturation, the MR behaves in the traditional electron–magnon model and matches well with the MR data from a- and c-axes with a slight offset, as seen in the SM. The decrease in resistivity along the b-axis is directly correlated with the TCS state, which persists to slightly past room temperature and is fully extinguished at 350 K, as seen in Fig. 1(d). There is a similar decrease in resistance along the a- and c-axes when the metamagnetic transition occurs ($\mu_0 H \geq 0.75T$), which is ascribed to a change in the magnetization from the FM-type state to another spin spiral state as seen in Fig. 1(b).

The component ρ_{high} corresponds to the applied magnetic field above $\mu_0 H \geq 0.75$ T. The high-field data in all three crystallographic directions can be fit to the Khosla–Fischer model, which describes electron–magnon scattering. The model describes the MR in systems with localized magnetic moments,

$$\rho_{high} = -b_1 \ln\left(1 + b_2^2(\mu_0 H)^2\right) + \frac{b_3^2(\mu_0 H)^2}{\left(1 + b_4^2(\mu_0 H)^2\right)}, \tag{3}$$

where the first term is the negative MR from electron–magnon scattering and the second term is the positive MR from orbital cyclotronic behavior. Below 50 K, there is a positive MR at high fields due to an orbital component that behaves semi-quadratically.[17] The value of the quadratic orbital cyclotronic behavior varies empirically and is corrected using a term in the denominator to fit the experimental data. The denominator term $[1 + b_4^2(\mu_0 H)^2]$ was originally proposed by Sondheimer and Wilson as a two-band model.[32] The values of each fitted value in all models are noted in the supplementary material, and b_1 and b_2 are noted in Figs. 2(g) and 2(h), respectively. The values for b_2, b_3, and b_4 correlate with the mobility and are proportional to the value of the field. These values are notably higher than expected for a ferromagnetic material at low temperatures, which indicates unique topology states.[28] At 50 K, the mobility noted by b_2 is close to $1000\ cm^2/(V\,s)$ along the c-axis, which has an MR of −12% at 9 T and 50 K. When used for the high-field data along the b-axis for $T < 75$ K, the pMR for this model normally resulting from an orbital cyclotronic component would give an unreasonable value for the mobility of $10^5\ cm^2/V\,s$ and is not considered further. We believe that the pMR along the b-axis is best described by the Rivier–Zlatic model, which describes the effect of localized spin fluctuations, whereas the Khosla–Fischer model proposes a similar quadratic fit from a third-order perturbation of the exchange Hamiltonian.[26,27]

The electron–magnon model correlating to $\rho = -b_1 \ln(1 + b_2^2(\mu_0 H)^2)$ is used solely for the data when T ≥ 50 K, which is below the phase transition at 68 K without an applied field, noted by a vertical gray line in the figure. The electron–magnon model includes a nonsaturating linear magnetoresistance when the applied field is larger than the saturation field of the structure. The metamagnetic material's properties behave as a ferromagnet in this field range, and the fitting parameters b_1 and b_2 are essentially the same when $T > T_1$ for all three crystallographic directions, which is marked by a vertical gray line at 116 K in the figure. The b_2 parameter, which correlates with the mobility of the carriers, decreases exponentially through the metamagnetic transition but then stabilizes to a constant value when the compound is in its helical spin spiral state for each crystallographic direction.

The MR measurements support the results in the magnetization measurements, and the large mobility indicates a unique topology of the structure.[10] In previous studies, a similar positive MR at low fields below a critical field was attributed to an electron-spin scattering of the s-d configurations in an antiferromagnetic metal.[20] When the field is parallel to the magnetization in the AFM state, it induces a positive MR below the critical field, which is around 0.75 T.[21] The intermediate

field can be considered the intermediate state below a secondary critical field, which changes with temperature due to the metamagnetic properties.[20] After the secondary critical field, the fluctuations are suppressed, leading to a negative MR similar to a pure FM.

In conclusion, the MR measurements along each crystallographic axis give more insight into the unique character of the Fe_3Ga_4 phases. At high fields beyond saturation, the MR matches with the electron–magnon and cyclotronic model proposed by Khosla–Fischer with the Sondheimer–Wilson correction for the exponent. At low fields, an anomalous and persistent positive MR emerges along the *b*-axis, accompanied by an uncharacteristically high mobility. This behavior suggests helical magnetic ordering that can generate a strong emergent field,[15] rather than the conventional FM ordering that was originally expected, potentially signaling topological phenomena. Future measurements may clarify whether a topological Hall effect (THE) is present in this compound.

See the supplementary material for this manuscript, which includes the crystallographic data and the magnetometry data with the transition temperatures for T_1 and T_2; all magnetoresistance data taken from 2.2–300 and 350–650 K; the derivative of MR vs temperature; and all fitting constants for the magnetoresistance.

Research at the United States Naval Academy was supported by the NSF DMR-EPM 1904446, Kinnear Fellowship, and the Office of Naval Research under Contract No. N0001423WX02132. Work at Northeastern University was partially supported by the National Science Foundation grant DMR-1905662 and the Air Force Office of Scientific Research award FA9550-20-1-0247 (D.H.). Work at VCU was partially funded by the National Science Foundation, Award No. 1726617. This work was also supported by the Office of Naval Research through the NRL basic research program. The National High Magnetic Field Laboratory was supported by the National Science Foundation through NSF/DMR-2128556 and DMR-1644779 and the State of Florida.

The views expressed in this article are those of the authors and do not reflect the official policy or position of the U.S. Naval Academy, Department of the Navy, the Department of Defense, or the U.S. Government.

AUTHOR DECLARATIONS

Conflict of Interest

The authors have no conflicts to disclose.

Author Contributions

Michelle E. Jamer: Conceptualization (lead); Data curation (lead); Formal analysis (lead); Funding acquisition (equal); Investigation (lead); Methodology (lead); Project administration (lead); Resources (lead); Supervision (lead); Validation (lead); Visualization (lead); Writing – original draft (lead); Writing – review & editing (lead). **Gregory M. Stephen:** Data curation (equal); Formal analysis (equal); Investigation (equal); Methodology (equal); Writing – review & editing (equal). **Brandon Wilfong:** Conceptualization (equal); Data curation (equal); Formal analysis (equal); Methodology (equal); Writing – review & editing (supporting). **Radhika Barua:** Methodology (supporting); Project administration (supporting); Resources (supporting); Writing – review & editing (supporting). **Frank M. Abel:** Investigation (equal); Methodology (equal); Writing – original draft (equal); Writing – review & editing (equal). **Steven P. Bennett:** Conceptualization (equal); Data curation (equal); Funding acquisition (equal); Writing – review & editing (equal). **Joseph C. Prestigiacomo:** Conceptualization (equal); Formal analysis (equal); Funding acquisition (equal); Writing – review & editing (equal). **Don Heiman:** Conceptualization (equal); Data curation (equal); Formal analysis (equal); Investigation (equal); Methodology (equal); Project administration (equal); Writing – original draft (equal); Writing – review & editing (equal). **David Graf:** Conceptualization (equal); Data curation (equal); Formal analysis (equal); Funding acquisition (equal); Investigation (equal); Methodology (equal); Project administration (equal); Resources (equal); Writing – review & editing (equal).

DATA AVAILABILITY

The data that support the findings of this study are available from the corresponding author upon reasonable request.

REFERENCES

[1]Z. Liu, Z. Feng, H. Yan, X. Wang, X. Zhou, P. Qin, H. Guo, R. Yu, and C. Jiang, "Antiferromagnetic piezospintronics," Adv. Electron. Mater. **5**(7), 1900176 (2019).
[2]L. Lewis, C. Marrows, and S. Langridge, "Coupled magnetic, structural, and electronic phase transitions in FeRh," J. Phys. D **49**, 323002 (2016).
[3]Z. Zhu, X. Yang, C. Cuimei, T. Shang, Y. Xie, and Z. Zhan, "Recent developments on the magnetic and electrical transport properties of FeRh- and Rh-based heterostructures," J. Phys.: Condens. Matter **34**, 144004 (2022).
[4]R. Barua, F. Jiménez-Villacorta, and L. Lewis, "Predicting magnetostructural trends in FeRh-based ternary systems," Appl. Phys. Lett. **103**, 102407 (2013).
[5]S. Bennett, A. Wong, A. Glavic, A. Herklotz, C. Urban, L. Valmianski, M. Biegalski, H. Christen, T. Ward, and V. Lauter, "Giant controllable magnetization changes induced by structural phase transitions in a metamagnetic artificial multiferroic," Sci. Rep. **6**, 22708 (2016).
[6]N. Blumenschein, G. Stephen, C. Cress, S. LaGasse, A. Hanbicki, S. Bennett, and A. Friedman, "High-speed metamagnetic switching of FeRh through joule heating," Sci. Rep. **12**, 22061 (2022).
[7]Z. Feng, H. Yan, and Z. Liu, "Electric-field control of magnetic order: From FeRh to topological antiferromagnetic spintronics," Adv. Electron. Mater. **5**, 1800466 (2019).
[8]N. Kawamiya and K. Adachi, "Magnetic and Mössbauer studies of metamagnetic Fe_3Ga_4," J. Phys. Soc. Jpn. **55**, 634 (1986).
[9]J. Mendez, C. Ekuma, Y. Wu, B. Fulfer, J. Prestigiacomo, W. Shelton, M. Jarrell, J. Moreno, D. Young, P. Adams *et al.*, "Competing magnetic states, disorder, and the magnetic character of Fe_3Ga_4," Phys. Rev. B **91**, 144409 (2015).
[10]B. Wilfong, A. Fedorko, D. R. Baigutlin, O. N. Miroshkina, X. Zhou, G. M. Stephen, A. L. Friedman, V. Sharma, O. Bishop, R. Barua, S. P. Bennett, D. Y. Chung, M. G. Kanatzidis, V. D. Buchelnikov, V. V. Sokolovskiy, B. Barbiellini, A. Bansil, D. Heiman, and M. E. Jamer, "Helical spin-density wave in room-temperature metallic antiferromagnet Fe_3Ga_4," J. Alloys Compd. **917**, 165532 (2022).
[11]J. C. Prestigiacomo, M. E. Jamer, P. G. Callahan, and S. P. Bennett, "Dual-component anomalous Hall effect in a helical spin-spiral metamagnet," Appl. Phys. Lett. **124**, 062409 (2024).
[12]B. Wilfong, V. Sharma, O. Bishop, A. Fedorko, D. Heiman, R. Barua, and M. E. Jamer, "The effect of vanadium substitution on the structural and magnetic properties of $(Fe_{1-x}V_x)_3Ga_4$," J. Magn. Magn. Mater. **563**, 169964 (2022).
[13]M. Afshar and I. I. Mazin, "Spin spiral and topological Hall effect in Fe_3Ga_4," Phys. Rev. B **104**, 094418 (2021).
[14]Y. Wu, Z. Ning, H. Cao, G. Cao, K. A. Benavides, S. Karna, G. T. McCandless, R. Jin, J. Y. Chan, W. Shelton *et al.*, "Spin density wave instability in a ferromagnet," Sci. Rep. **8**(1), 5225 (2018).

[15]P. R. Baral, V. Ukleev, I. Živković, Y. Lee, F. Orlandi, P. Manuel, Y. Skourski, L. Keller, A. Stunault, J. A. Rodríguez-Velamazán *et al.*, "Fluctuation-driven topological hall effect in room-temperature itinerant helimagnet Fe_3Ga_4," Nat. Commun. **16**, 3898 (2025).
[16]M. Philippe, B. Malaman, B. Roques, A. Courtois, and J. Protas, "Structures cristallines des phases Fe_3Ga_4 et Cr_3Ga_4," Acta Crystallogr., Sect. B **31**, 477 (1975).
[17]N. A. Porter, J. C. Gartside, and C. H. Marrows, "Scattering mechanisms in textured FeGe thin films: Magnetoresistance and the anomalous Hall effect," Phys. Rev. B **90**, 024403 (2014).
[18]P. Saha, V. Nagpal, P. Das, and S. Patnaik, "Dominance of electron-magnon scattering in itinerant ferromagnet Fe_3GeTe_2," arXiv:2209.03555 (2022).
[19]S. Murayama and H. Nagasawa, "Magnetoresistance in antiferromagnetic α-Mn metal," J. Phys. Soc. Jpn. **43**, 1216 (1977).
[20]H. Yamada and T. Satoshi, "Magnetoresistance of antiferromagnetic metals due to *s-d* interaction," J. Phys. Soc. Jpn. **34**, 51 (1973).
[21]H. Nagasawa, "Magnetoresistance of neodymium metal," Phys. Lett. A **41**, 39 (1972).
[22]A. Azarevich, V. Glushkov, S. Demishev, A. Bogach, V. Voronov, S. Gavrilkin, N. Shitsevalova, V. Filipov, S. Gabáni, J. Kačmarčík, K. Flachbart, and N. Sluchanko, "Evidence of symmetry lowering in antiferromagnetic metal TmB_{12} with dynamic charge stripes," J. Phys.: Condens. Matter **34**, 065602 (2022).
[23]S. Arajs and G. R. Dunmyre, "Electrical resistivity and transverse electrical magnetoresistivity of chromium," J. Appl. Phys. **36**, 3555 (1965).
[24]M. Naito and S. Tanaka, "Galvanomagnetic effects in the charge-density-wave state of 2*H*-$NbSe_2$ and 2*H*-$TaSe_2$," J. Phys. Soc. Jpn. **51**, 228 (1982).
[25]Y. Feng, Y. Wang, D. Silevitch, J.-Q. Yan, R. Kobayashi, H. Masato, T. Nakama, Y. Onuki, A. Suslov, B. Mihaila, P. Littlwood, and T. Rosenbaum, "Linear magnetoresistance in the low-field limit in density-wave materials," Proc. Natl. Acad. Sci. U. S. A. **116**, 11201 (2019).
[26]V. Zlatic, "Low temperature magnetoresistance of nearly magnetic transition metal-based alloys and actinides," J. Phys. F **8**, 489 (1978).
[27]V. Zlatic, "Low-temperature magnetoresistance of $CeAl_3$," J. Phys. F **11**, 2147 (1981).
[28]Y. He, J. Gayles, M. Yao, T. Helm, T. Reimann, V. Strocov, W. Schnelle, M. Nickals, Y. Sun, G. Fecher, and C. Felser, "Large linear non-saturating magnetoresistance and high mobility in ferromagnetic MnBi," Nat. Commun. **12**, 4576 (2021).
[29]M. Lee, W. Kang, Y. Onose, Y. Tokura, and N. P. Ong, "Unusual Hall effect anomaly in MnSi under pressure," Phys. Rev. Lett. **102**, 186601 (2009).
[30]N. Kanazawa, Y. Nii, X. Zhang, A. Mishcehnko, G. De Filippis, F. Kagawa, Y. Iwasa, N. Nagaosa, and Y. Tokura, "Critical phenomena of emergent magnetic monopoles in a chiral magnet," Nat. Commun. **7**, 11622 (2016).
[31]N. Nagaosa and Y. Tokura, "Topological properties and dynamics of magnetic skyrmions," Nat. Nanotechnol. **8**, 899 (2013).
[32]E. Sondheimer and A. Wilson, "The theory of the magneto-resistance effects in metals," Proc. R. Soc. Ser. A **190**, 435 (1947).